Graphene and 2D Materials (2024) 9:59–76
https://doi.org/10.1007/s41127-023-00071-5

ORIGINAL ARTICLE

Novel electrically conductive electrospun PCL-MXene scaffolds for cardiac tissue regeneration

Kateryna Diedkova[1,2] · Yevheniia Husak[1,3] · Wojciech Simka[3] · Viktoriia Korniienko[1,2] · Bojan Petrovic[4] · Anton Roshchupkin[1] · Agnieszka Stolarczyk[3] · Natalia Waloszczyk[3] · Ilya Yanko[1] · Kaspars Jekabsons[2] · Maria Čaplovičová[5] · Alexander D. Pogrebnjak[1,6] · Veronika Zahorodna[7] · Oleksiy Gogotsi[7] · Iryna Roslyk[7] · Ivan Baginskiy[1,7] · Marko Radovic[8] · Sanja Kojic[9] · Una Riekstina[2] · Maksym Pogorielov[1,2]

Received: 14 July 2023 / Revised: 29 November 2023 / Accepted: 3 December 2023 / Published online: 28 December 2023

Abstract

Effective cardiac tissue regeneration necessitates scaffolds that mimic the native extracellular matrix and possess desirable properties, such as electrical conductivity and biocompatibility. The choice of an appropriate fabrication method is paramount in achieving reproducibility, scalability, and rapid production of cardiac tissue patches. Electrospinning, a versatile and widely utilized technique, offers precise control over fiber diameter, pore size, and alignment, rendering it an ideal method for creating intricate cardiac scaffolds. In light of the limitations of existing therapies and the need for innovative approaches, this research aims to explore the development of novel patches for cardiac tissue regeneration. By investigating the integration of MXenes into electrospun polycaprolactone (PCL) membranes, we aim to harness the unique properties of MXenes to create conductive, biocompatible, and mechanically robust scaffolds that promote cell adhesion, proliferation, and functional maturation. The application of oxygen plasma treatment enhances the infiltration of MXene into the PCL electrospun membrane, significantly reducing the surface contact angle and promoting cell adhesion. Regardless of the number of MXene deposition repetitions, all variants demonstrated strong biocompatibility and supported the formation of cell symplasts after fibroblast seeding. The remarkable electrical conductivity of PCL-MXene membranes, coupled with the positive biological outcomes presented in this study, has the potential to drive significant advancements in the field of cardiac tissue engineering. This research offers fresh insights and approaches to tackle the challenges associated with myocardial repair and regeneration.

Keywords MXene · PCL · Electroconductive electrospun membrane · Oxygen plasma treatment · Tissue regeneration

Una Riekstina and Maksym Pogorielov are co-last authors.

✉ Maksym Pogorielov
maksym.pogorielov@lu.lv

[1] Sumy State University, 2 Rymskogo-Korsakova St, Sumy 40007, Ukraine

[2] University of Latvia, 3 Jelgavas St, Riga 1004, Latvia

[3] Faculty of Chemistry, Silesian University of Technology, 9 Strzody St, 44-100 Gliwice, Poland

[4] Faculty of Medicine, University of Novi Sad, Hajduk Veljkova 3, 21000 Novi Sad, Serbia

[5] Centre for Nanodiagnostics of Materials, Slovak University of Technology in Bratislava, 5 Vazovova St, Bratislava 812 43, Slovakia

[6] Faculty of Material Science in Trnava, Institute of Materials, Slovak University of Technology in Bratislava, Jana Bottu c2781/25, Trnava, Slovakia

[7] Materials Research Centre, 3 Krzhizhanovskogo St, Kyiv 03142, Ukraine

[8] University of Novi Sad, BioSense Institute, Dr Zorana Djindjica 1, 21000 Novi Sad, Serbia

[9] Faculty of Technical Sciences, University of Novi Sad, Trg Dositeja Obradovića 6, 21000 Novi Sad, Serbia

1 Introduction

Cardiovascular diseases (CVD) still remain one of the leading causes of both morbidity and mortality worldwide and cause a significant burden for national healthcare organizations [1]. Thus, the UK health care cost for both treatments of CVD and economic loss due to premature deaths, disability, and informal care is approximately £30 billion per year [2]. Despite significant progress in CVD treatment strategy, including the pharmaceutical sector and surgical intervention, tissue engineering could substantially improve success in the rehabilitation and treatment of patients with affected myocardial tissue [3]. To ensure complete acceptance by the host tissue, the implants must mimic as much as possible the biological environment porosity, permeability, and mechanical stability. Additionally, grafts should meet specific requirements depending on host tissues. The cardiac muscle is the second largest electrically active infrastructure in our body after nervous tissue [4]. Therefore, materials that interface with electrically active tissues for cardiovascular purposes must also be conductive to enhance the biological response to external stimuli.

Nowadays, different strategies, including cell-based or cell-free therapies combined with tissue engineering approaches, offer a promising technology by the development of three-dimensional biomimetic conductive scaffolds for heart tissue replacement [5, 6]. Two main strategies are used for cardiac tissue engineering: (1) fabrication of organic conductive polymers and (2) incorporation of conductive particles in polymeric matrix [7].

The first electroconductive scaffolds for heart tissue engineering were based on conductive polymers: polypyrrole (PPy), polyaniline (PANI), and poly(3,4-ethyl-enedioxythiophene) (PEDOT) [3]. Low biocompatibility, possible inflammatory response, and toxic degradation products limited the wide application of these materials. To provide a more favorable biological response, a novel strategy of biocompatible polymer doped with conductive materials was introduced. Gold- and carbon-based nanoparticles are the most widely used conductive nanomaterials for cardiac tissue regeneration purposes. You et al. demonstrated proper cell adhesion and viability of neonatal rat cardiomyocytes on thiol-2-hydroxyethyl methacrylate (thiol-HEMA) scaffolds, containing homogeneously distributed gold nanoparticles [8]. Some research revealed possible differentiation of the chorion-derived mesenchymal stromal cells (MSCs) into cardiomyocytes on gold-coated collagen fibers with electrical stimulation [9]. Later, Ravichandran et al. showed the same effect of both low and high concentrations of gold nanoparticles in electrospun bovine serum albumin (BSA)/polyvinyl alcohol (PVA) scaffold with no difference in proliferation and cytoskeleton gene expression [10]. But Baei et al. demonstrated that only 2% of gold nanoparticles in chitosan electrospun scaffold possessed more capability for cardiogenic differentiation of MSCs [11]. A high concentration of gold could lead to inflammatory complications and provide a cytotoxic effect on surrounded tissue that limited gold nanoparticle application. In contrast, carbon-based nanomaterials demonstrate a better biological profile and exhibit advanced conductivity with better mechanical properties. Thus, Sherrell et al. showed that single-walled nanotubes (SWNT)–collagen–chitosan hydrogel can provide sufficient mechanical support and promote cell survival, proliferation, and differentiation as well as improvement in physiological properties [12]. Other studies demonstrated significant effectiveness of polycaprolactone–silk fibroin–SWNT hydrogel [13], SWNT–alginate–methacrylated collagen 3D-printed scaffold [14], and poly(octamethylene maleate (anhydride) 1,2,4-butanetricarboxylate)–SWNT composite [15]. Graphene-based materials, such as PCL–graphene electrospun fibers [16], injectable hydrogel composed graphene–hyaluronic acid [17], and graphene–PEG hybrid scaffolds [18], also demonstrated good remarkable conductivity, mechanical properties, and biocompatibility. But, despite the positive *in vitro* study, graphene-based materials could possess genotoxicity and not degrade *in vivo*.

Numerous electrically responsive polymers, combined with conductive doping agents, have been employed in the development of electrically conductive scaffolds. These scaffolds have consistently demonstrated encouraging biological outcomes at the cellular and tissue levels, including aspects such as biocompatibility, cell proliferation, tissue healing, and regeneration [19–22]. These attributes position them as viable contenders for use in regenerative applications, with promising outcomes. Nevertheless, the integration of electrical stimulation in conjunction with these materials and their progression to *in vivo* studies remains relatively limited [23]. These limitations required the development of novel approaches for material design. Transition metal carbides, nitrides, and carbonitrides (MXenes), discovered by Yury Gogotsi, Michel Barsoum, and co-workers in 2011, are a fast-growing family of 2D materials that demonstrated major applications in cancer treatment, bacteriology, immunology, target drug delivery, tissue engineering, etc., and, due to remarkable electroconductive properties, possess promising materials for conductive tissue regeneration [24]. Recent research demonstrates high biocompatibility and *in vivo* safety for different applications that meet major criteria for tissue engineering additives [25–27]. Notably, MXenes have demonstrated the ability to facilitate cell adhesion and proliferation, critical factors in tissue regeneration. Their surface properties offer a favorable environment for

cellular interactions, promoting the development of functional tissue interfaces [22]. Furthermore, the tunable surface chemistry of MXenes allows for modifications that can enhance their biocompatibility, tailoring them to specific tissue types. Immunocompatibility, another crucial facet, pertains to a material's capacity to elicit immune responses. MXenes have exhibited limited immunogenicity, suggesting a potential for reduced adverse reactions when integrated into biological systems [28–30]. This characteristic is pivotal for minimizing inflammatory responses and fostering a harmonious coexistence between the material and the host. Some recent studies have already demonstrated the possible application of MXene for development of flexible interfaces that have potential clinical utility for multiscale epidermal sensing and neuromodulation [31] and for remote, nongenetic, optical modulation of neuronal electrical activity [32]. Compared to other 2D materials commonly used in tissue engineering, MXenes stand out due to their exceptional electrical conductivity [33], which can promote enhanced cell signaling and communication within tissue constructs [34]. This unique property makes MXenes particularly promising for applications involving electrically active tissues. Unlike some other 2D materials, MXenes possess a layered structure with readily accessible surface functional groups [35, 36]. This feature allows for easy grafting of bioactive molecules, making MXenes an ideal choice for engineering scaffolds that can mimic the natural extracellular matrix and provide a conducive microenvironment for cell adhesion and growth. But there are no data about development of a full-scale scaffold for cardiac or neural tissue engineering based on MXene. Polycaprolactone (PCL) is currently under investigation as a potential framework for vascular and myocardial regeneration. This interest is attributed to its straightforward production process, favorable mechanical, chemical, and biocompatible characteristics, and notably, its capacity to degrade naturally. These qualities render it a promising candidate for rejuvenating and reconstructing heart function following instances of disease or injury [37, 38]. Recently, we have demonstrated the possibilities of PCL-MXene electrospun fiber formation with high conductivity and appropriate host response [39–41]. PCL, despite the suitable biocompatibility, safety, and biodegradation abilities, demonstrates high hydrophobic properties that limit the assembly of MXene (or other nanoparticles and nanolaminates) on the electrospun membrane and required post-treatment, particularly with H_2SO_4 or NaOH solutions that increase risk of residuals release during the degradation period with unpredicted adverse effects. To overcome the current limitation, in current research, we provide oxygen plasma treatment of electrospun PCL mats followed by multilayer MXene assembly with structural, functional, and biological characterizations with the aim of cardiac tissue engineering patches development. The innovative technique employed in this study enables the achievement of a uniform distribution of MXene throughout the PCL mats, while causing minimal alterations to the electrospun material's structure. The remarkable electrical conductivity exhibited by the novel MXene-infused material (elevating conductivity from 5.22 to 326.33 mS/m) is complemented by a favorable cellular response. This remarkable combination of attributes paves the way for the advancement of highly efficient tissue engineering scaffolds, holding significant promise for cardiac and vascular tissue regeneration applications.

2 Materials and methods

2.1 Production PCL electrospun membrane

Polycaprolactone (PCL), Mn = 80,000 g/mol, was obtained from Sigma-Aldrich (Saint Louis, MI, USA). Chloroform (purity ≥ 99%) was purchased from Chempur (Piekary Śląskie, Poland), and *N*, *N*-Dimethylformamide (DMF) (purity ≥ 99%) was derived from Honeywell (Charlotte, North Carolina, US).

To prepare the electrospinning solution, 0.96-g polycaprolactone was wholly dissolved in an 8-mL solvent (a mixture of chloroform and DMF, with the ratio of 3:1) by 3-h stirring at 300 rpm on a magnetic stirrer at room temperature [42, 43]. The polymeric solution was transferred in 5-mL glass syringe (with an inner diameter of needle 0.8 mm). Electrospun fiber mats were produced by the conventional method of electrospinning with the following parameters: 17-kV power, 170 mm from the tip to a collector, a feeding rate of 1 mL/h, and a drum (7 cm in diameter) rotating speed of 350 rpm.

2.2 MXene synthesis

$Ti_3C_2T_x$ MXene (T is OH, Cl, or F) was synthesized using a modified etching method known as MILD. Details of MXene slurry synthesis are described in the previous research [42]. To obtain a water-based colloidal solution of Ti_3C_2 flakes, the wet MXene slurry was further subjected to a delamination process. This process aimed to separate the Ti_3C_2 flakes into individual layers in a colloidal form with pH 7.0. As a final result, we obtained MXene solution in concentration of 4.4 mg/mL with Ti_3C_2 lateral size from 1 to 2 µm.

2.3 MXene deposition on PCL scaffolds

The PCL membranes were soaked in MXene solution with a 4.4-mg/mL concentration. The MXene solution was sonicated for 1 min in an ultrasonic bath with a power of 50 W at 40 kHz. Polycaprolactone is known to be a hydrophobic polymer; therefore, PCL scaffolds (Ø 5 mm

in diameter) were treated with oxygen plasma (K1050X Plasma Asher (Kent, UK)) for 2 min at 15 Watts that improves the hydrophilic properties of the PCL surface. As-treated PCL scaffolds were put in small containers (20 mL) with 5 mL of the MXene solution. The container was filled with argon to prevent the oxidation of MXenes. The container with membranes was sonicated for 5 min in an ultrasonic bath with 50 W at 40 kHz and left for 3 h to let MXene soak into the PCL scaffold. Then, the PCL scaffolds were removed from the MXene solution, washed in DI water to remove excess of the solution, and dried on filter paper overnight. This procedure was repeated 2 times to obtain PCL membranes with different layers of MXene. To increase the hydrophilic properties of the PCL-MXene, nanocomposite scaffolds were additionally treated with oxygen plasma and denoted as PCL-MX1-PL, PCL-MX2-PL, and PCL-MX3-PL.

2.4 Scanning electron microscopy with EDX and transmission electron microscopy

The surface morphology of the membranes was characterized by scanning electron microscopy (SEM, Phenom ProX, Phenom-World BV, the Netherlands) which was equipped with an energy-dispersive X-ray spectrometer (EDX). The microscope operated at an accelerating voltage (Uacc) of 15 kV. To prove the MXene deposition on PCL fiber, HRTEM characterization was performed using double corrected analytical scanning transmission electron microscope JEOL JEM-ARM200CF at 200 kV. TEM images were recorded by a bottom mounted CCD camera Gatan Ultrascan 1000 XP with a resolution of 2048 × 2048 pixels using the Digital Micrograph 3.43 SW package (Gatan, USA).

3 Cross-section with*EDX membranes*

The membranes were cut to yield a cross-section. The cross-section morphology and chemical composition of the samples were observed by SEM and by EDX line scan (Fig. 1). Samples were fixed by EM-Tec S-Clip sample holder with 1xS-Clip at 90°.

3.1 Three-dimensional visualization of membranes

Three-dimensional images and submicrometer roughness measurements of the samples were generated by the Phenom desktop scanning electron microscope. Based on "shape from shading" technology, 3D imaging was used for helping to interpret sample characteristics. The roughness characteristics were presented via the average roughness (*Ra*) and the roughness height (*Rz*).

3.1.1 Membrane degradation

The degradation of materials was assessed in a PBS solution as follows: Static degradation of samples was conducted at a temperature of 37 °C and pH 7.4 to simulate *in vitro* degradation conditions. Samples with pre-determined weights were immersed in a sterile PBS solution for 7 days. Subsequently, they were retrieved, rinsed with distilled water, and weighed to assess water absorption (at the 1st and 4th week). They were then dried for 12 h and weighed again to evaluate weight loss. The PBS solution was changed every 3 days. This procedure was repeated in the 1st, 2nd, 3rd, and 4th weeks. The weight loss of the sample was calculated using the following formula:

$$\%\text{Mass loss} = \left(\frac{Wo - Wd}{Wo}\right) \times 100$$

where *Wo*—initial weight of sample and *Wd*—sample weight after degradation time point.

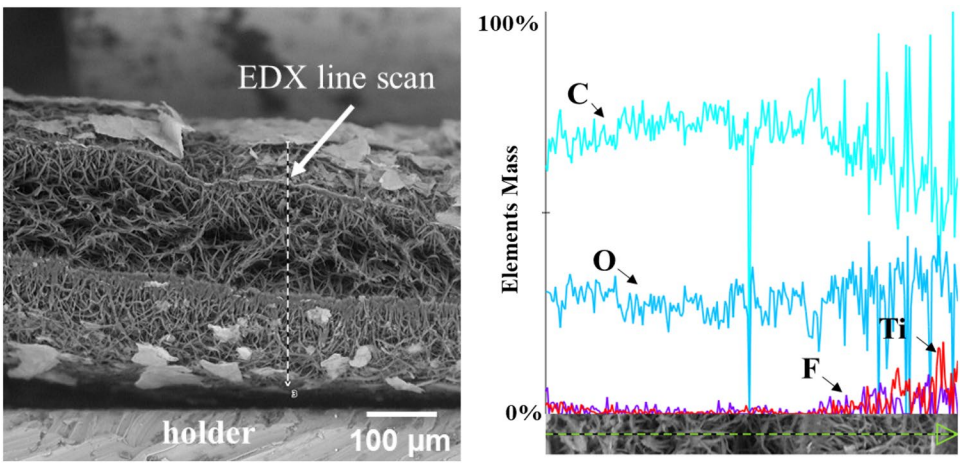

Fig. 1 Scanning electron microscopy image of PCL-MXene membranes cross-section (left side) with the representation of EDX line (dotted line) and example of cross-sectional EDX elements line scan (right side)

To assess dynamic degradation, we employed the setup illustrated in Supplement, Fig. S1. Samples with a diameter of 5 mm were placed in containers (B), and a sterile PBS solution was circulated from the reservoir (D) through the samples, passing through a filter (C), and returning to the container. The flow rate was set at 0.8 mL per minute, corresponding to myocardial blood flow [44]. Every 3 days, a fresh sterile PBS solution was added to reservoir D. The entire degradation procedure was conducted at 37 °C in a thermostat (E). Weight loss was determined using the same methodology and at the same time intervals as in static degradation.

3.1.2 FTIR and Raman measurements

Fourier transform infrared (FTIR-ATR) spectra were recorded using a Nicolet iS10 spectrometer (Thermo Fisher Scientific Inc., USA), equipped with a diamond attenuated total reflectance (ATR) sampling accessory. Spectra were collected for a range of 600–2350 cm^{-1} using a mercury cadmium telluride (MCT) detector.

Raman spectra were recorded using an InVia confocal Raman spectrometer from Renishaw (UK) equipped with a DM2500 microscope from Leica. The excitation source was a helium–neon gas laser (632.8 nm). A diffraction grating with 1200 lines/mm was used for the measurements. During the Raman analyses, 1% of the maximum laser power was used. For measurements conducted using a 50× objective lens, this translated to an effective power of 7.6 mW for a 632.8-nm laser. The detector was a camera with a high-resolution charge-coupled device (CCD) matrix. All samples were analyzed without pretreatment. Raman spectra were recorded in the range of 140–2000 cm^{-1}. Measurements were performed with an exposure time of 5 s and an accumulation number of 5 spectra. For each sample, the measurement was performed at least 3 times, in different, randomly selected locations. A 50× magnifying Leica lens was used to focus on the surface of the sample (N.A. lens numerical aperture = 0.75), for which the size of the laser beam interacting with the sample is approx. 2 µm.

3.1.3 Measurement of contact angle

Membrane surface wettability was measured with 2-µL droplets of deionized water using a video-based optical contact angle measuring equipment OCA 15 EC, Series GM-10-473V-5.0 (Data Physics, Filderstadt, Germany). Static and dynamic contact angles were used to evaluate the hydrophobicity/hydrophilicity of a solid surface. The values of the static and dynamic contact angles point to different properties of the substrates. First, we measured the static contact angles when the droplet was standing on the surface. The camera fixes the moment of the first interaction between water and the surface of the membrane, and it is expressed as the constant contact angle and, accordingly, the instant wetting characteristics of the substrate. In contrast, the dynamic investigation allows observing the wetting process of the surface through time. In this case, the camera fixed the values of the contact angle interaction between the surface and distilled water over a particular time. Thus, this measured the dynamics of the absorption of a water droplet by the membranes and recorded the dynamic changes in its shape. The wettability values were measured on three different membranes, and an average of three readings was reported for each sample.

3.1.4 Electrical conductivity

Resistance measurements are performed with a digital multimeter (EX350, EXTECH, Nashua, New Hampshire, US). Samples were connected with probes at a 1-cm distance between them. There were eight sample types, three of each group. Each sample was measured at least 3 times with a repeatable process of probe connection for each measurement. Each sample type was measured at least 10 times in total. Conductivity is recalculated afterward.

3.1.5 Biocompatibility

The human dermal fibroblasts (D6P10) (Ethics committee for research in life sciences and medicine of the UL approval No. 71-35/17) were used for the assessment of cytotoxicity and biocompatibility of samples. Materials were sterilized by immersion in 70% ethanol for 1 h. Afterward, membranes were washed with phosphate-buffered saline (PBS) 3 times for 5 min to eliminate any ethanol residuals. Before the experiment, D6P10 dermal fibroblasts were grown in 75-cm^2 cell culture flasks under standard culture conditions of humidified air containing 5% CO_2 at 37 °C with medium renewal every 2–3 days. Dulbecco's modified Eagle medium/nutrient mixture F-12 (DMEM/F-12) with L-glutamine was used, containing 100 units of penicillin, 100 units of streptomycin, 2.5 of amphotericin B per mL, and 10% fetal bovine serum. All cell culture reagents were purchased from Sigma-Aldrich, USA. The circular samples Ø 5 mm were placed on a 96-well plate (Sarstedt), and dermal fibroblasts were seeded on membranes at a density of 10^4 cells/cm^2 with the addition of complete cell culture media. Cells seeded into wells without membranes served as a positive control, and the medium without cells and membranes was a negative control. The Alamar blue colorimetric assay assessed cell adhesion at 24 h and cell proliferation on the 3rd and 7th day. Alamar blue (Sigma-Aldrich, USA) was added to each well equal to 10% of the medium volume. The Alamar blue solution was also added to the negative and positive controls. The plates were incubated for 8 h

at 37 °C in the incubator. The absorbance was measured using a microplate reader Tecan Infinite M200 Pro (Tecan Trading AG, Switzerland) plate reader at wavelengths of 570–600 nm. The cells were quantified at different time intervals: 1, 3, and 7 days. For each sample, there were triple repetitions.

After the final day, samples were washed with PBS twice and fixed with a 3.5% formaldehyde solution (Sigma-Aldrich) for 10 min. After fixation, the cells were permeabilized to improve staining results by a solution consisting of 1% BSA and 0.1% Triton X-100 diluted in PBS. The cell cytoskeleton was stained by ActinRed 555 (Thermo Scientific, USA), and the nuclei of the dermal fibroblasts were stained by Hoechst 33342 (Thermo Scientific, USA) diluted 1:1000. After that, all samples were analyzed with a fluorescence microscope (Nikon Eclipse TI Fluorescence Microscope, Japan) in the DAPI and TRITC channels.

3.1.6 Antibacterial properties

The electrospun PCL fibers were fabricated into membranes with a diameter of 0.5 cm. To ensure sterilization, the membranes were immersed in 70% ethanol for half an hour. Subsequently, the samples underwent three consecutive rinses in saline for 5 min each to eliminate any residual ethanol. Gram-positive (*Staphylococcus aureus*) and gram-negative (*Escherichia coli*) bacteria were used in the experiment. The isolates were grown in Mueller–Hinton broth (MHB) at 37 °C in a thermostat overnight. The cultures were diluted to a cell concentration of 10^5 CFU/mL using a densitometer and nutritional media.

In a 96-well plate, each well was loaded with 150 µL of overnight culture containing 10^5 CFU/mL. The test and control membranes were then inserted into the plate and allowed to come into contact with the bacterial cultures for 4, 6, 8, and 24 h. Following the incubation period, the membranes were gently rinsed with PBS to remove loosely adherent bacteria. Subsequently, the samples were transferred to 1.5-mL Eppendorf tubes containing 150 µL of nutritional broth and sonicated for 1 min in an ultrasonic bath operating at 50 W and 40 kHz to detach the bacteria from the membrane surface.

3.1.7 Bacteria proliferation assay

The bacterial suspension that was obtained previously was utilized to assess the overall metabolic activity of bacteria present on the membrane surface. The resazurin reduction assay, employing a commercially available resazurin solution (CellTiter-Blue, CTB, Promega, Madison, WI, USA), was employed to evaluate the metabolic activity of the bacteria. The resazurin reagent was added at a concentration of 10% v/v to each well, and the plates were placed in a microplate thermoshaker, shaken, and incubated at 37 °C for 2 h. Subsequently, the optical density (absorbance) was measured at 570–600 nm using a Multiskan FC plate reader (Thermo Fisher Scientific). The obtained results were quantified using a formula derived from the Method for Measuring Cytotoxicity or Proliferation Using AlamarBlue by Spectrophotometry (Bio-Rad Laboratories). The experiment was conducted in triplicate.

3.1.8 Scanning electron microscopy membranes with bacteria

After the completion of the bacterial proliferation assay, the samples were prepared for scanning electron microscopy (SEM) imaging. Initially, the samples were fixed in freshly prepared 2.5% glutaraldehyde solution in PBS for 30 min at room temperature. The glutaraldehyde solution was then removed, and the wells were washed with PBS for 15 min. The subsequent dehydration process involved sequential immersion in ethanol at increasing concentrations (30%, 50%, 70%, 90%, and 96%) for 30 min each, followed by overnight incubation in 96% ethanol. After dehydration, ethanol was removed, and the samples were air-dried at room temperature. To enhance conductivity and image quality, a silver coating was applied to the samples. Scanning electron microscopy (SEM) was performed using an SEO-SEM Inspect S50-B instrument. Images of each sample were captured at fixed magnifications and settings.

4 Results

4.1 Structural properties of PCL-MXene membrane

The as-spun PCL membrane consists of randomly oriented fibers with varying diameters, ranging from $\leq$0.5 to 2 µm. The fiber diameter distribution reveals a predominance of thin fibers ($\leq$0.5 µm) with a frequency exceeding 80% (see Fig. 2). The random fiber orientation results in numerous interconnected pores within the membrane, with porous area fractions ranging from $\leq$0.5 to 2 µm^2. Small pores make up the majority (87.6%) of the total pore volume. To enhance the hydrophilicity of the membrane prior to MXene deposition, oxygen plasma treatment was employed. This treatment did not significantly alter the structural properties of the material but led to changes in the distribution of fiber diameters and porous area fractions. Specifically, the treatment removed thin fibers and increased overall porosity. The latter parameter is critical for achieving uniform MXene distribution within the inner layers of the PCL membrane, as the size of MXene flakes (1–2 µm) does not align with the initial porosity of the PCL mats. Furthermore, the presence of larger pores (10–20 µm) is vital for cell attachment and

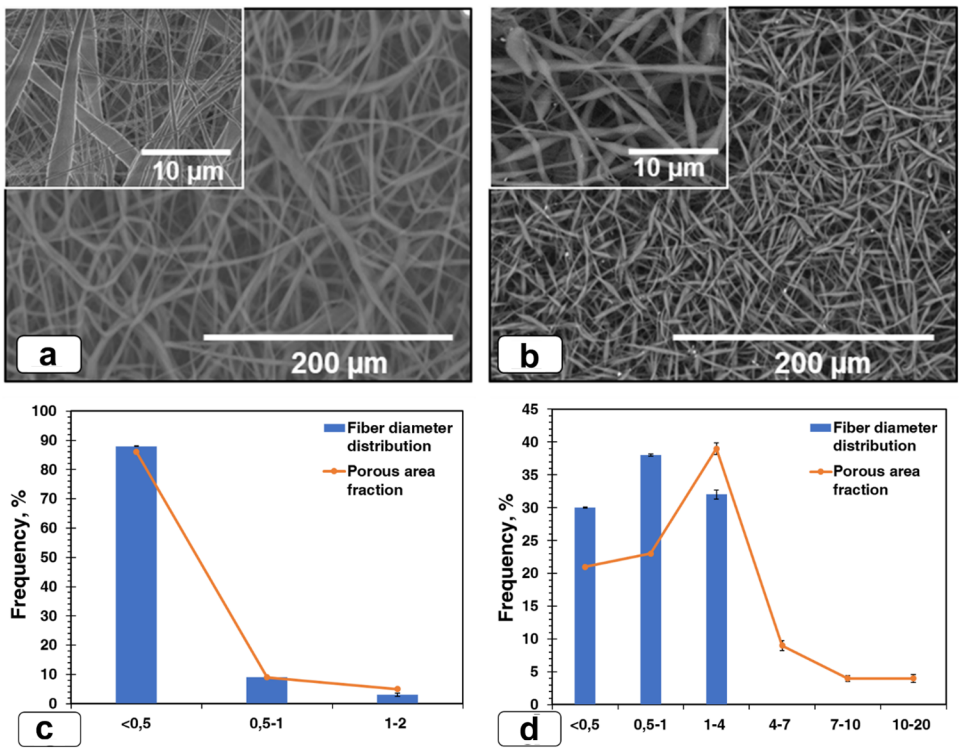

Fig. 2 Scanning electron microscopy images with frequency of "fiber diameter distribution" (µm) **c** and "porous area fraction" (μm^2) **d** value (diagrams below the corresponding SEM image) of electrospun membranes before **a** and after **b** oxygen plasma treatment. The magnification of the main images is ×500 (scale bar = 200 µm) and on the insets—×5000 (scale bar = 10 µm)

migration, making the membrane suitable for tissue engineering applications [45].

MXene deposition slightly alters the structure of PCL membranes, which is visually apparent in SEM images as a spiderweb-like pattern (Fig. 3a–c). The number of deposition procedures directly affects the fiber diameter and the fraction of porous area, as depicted in the diagrams of Fig. 3 (upper diagram): This leads to a significant increase in fiber diameter and slight decrease in porosity. HRTEM demonstrated the integration of MXene flakes on PCL fiber (Insertions of Fig. 3a and d). Our previous research has demonstrated that MXenes cover individual PCL fibers, significantly impacting their thickness and decreasing the porous area fraction [42]. Interestingly, oxygen plasma treatment of PCL-MXene membranes does not significantly alter the structural properties of the material (Fig. 3d–f), but it does lead to a reduction in fiber diameter. The fiber diameter distribution diagram (Fig. 3, low diagram) illustrates a leftward shift in the frequency of diameters compared to the non-treated PCL-MXene membranes. These changes considerably increase the porosity of the membranes, although there is no substantial difference observed between one coating and two or three depositions.

Additionally, EDS mapping (Supplement, Figs. S2 and S3) demonstrates a uniform distribution of Ti throughout the PCL membranes, providing evidence of $Ti_3C_2T_x$ MXene deposition. The EDS spectra reveal an increase in the atomic percentage of Ti from 2.45% after one deposition to 5.79% after three deposits. Oxygen plasma treatment does not affect the distribution of Ti but slightly reduces its concentration on the membrane surface (1.97% after one deposition and 4.00% after three depositions). This phenomenon is likely attributed to removing the Ti layer from the surface by introducing additional oxygen groups during plasma treatment.

The SEM images of PCL-MXene membrane cross-sections demonstrated randomly oriented fibers that create interconnected pores. It is important to note that the innermost layer of the material consists of a dense, non-porous membrane, which is likely a result of PCL melting during the electrospinning process. The high porosity of the membrane allows for deep penetration of MXenes; however, the inner layers are not filled with 2D flakes (Fig. 4a–c). The first coating only deposits MXenes on the superficial layers, while two or three repetitions enable deeper penetration, accounting for approximately 30–40% of the membrane thickness. EDX line measurements showed an increasing atomic percentage of Ti (the main component of MXene) with an increase in coating repetitions (from 18.7 to 49.1% in the PCL-MX group). Additionally, a decrease in the Ti gradient from the surface to the internal part of the membrane indicates a lack of MXene deposition in the deep layers. It is worth noting that plasma pretreatment facilitated MXene penetration more effectively compared to previously developed chemical (acid and alkali) pretreatments [40, 41]. Oxygen plasma treatment did not impact the internal structural properties of the PCL-MXene membranes. In contrast with the EDS data from the surface, plasma treatment did not affect the distribution of Ti inside the membrane or the

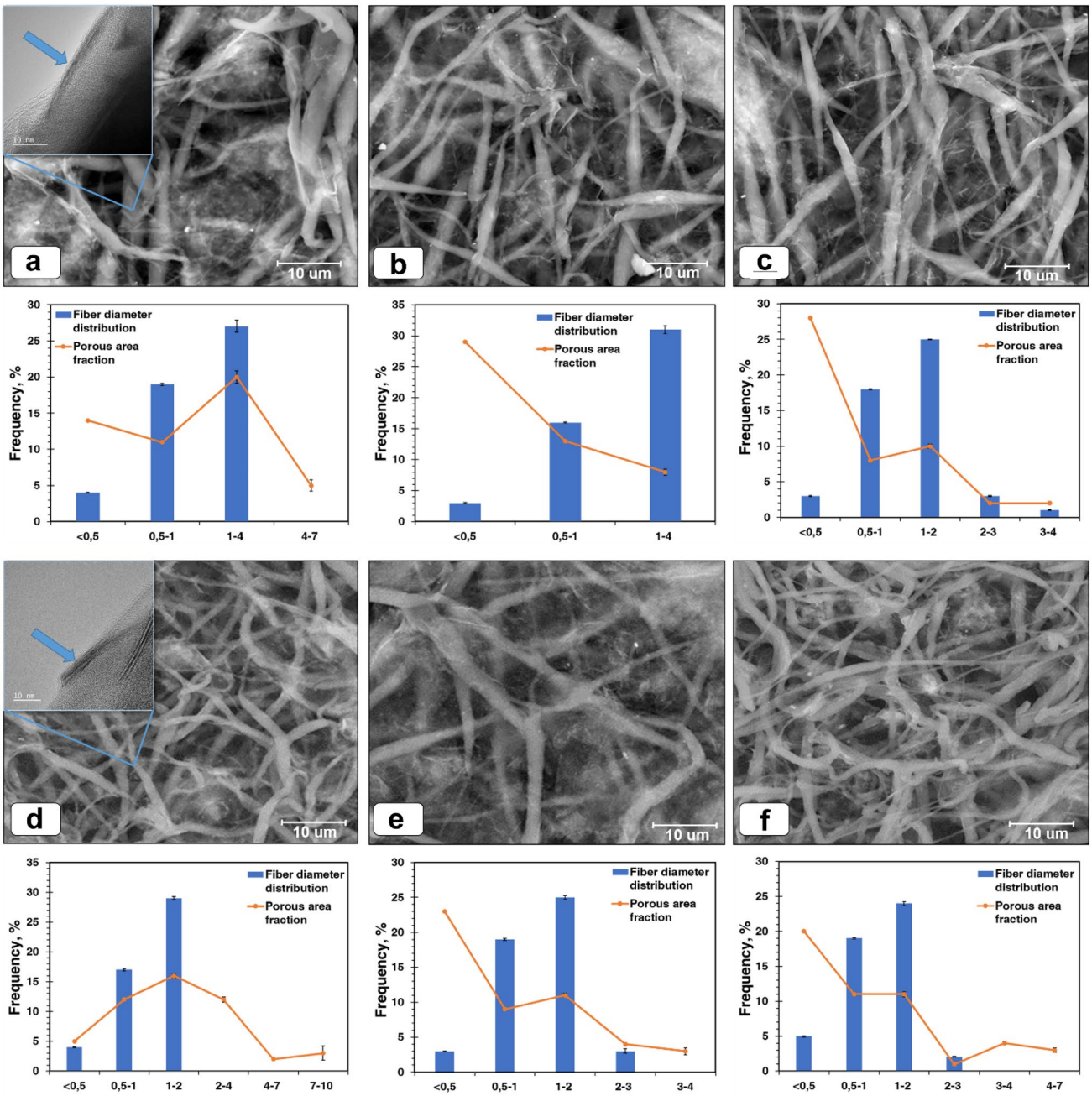

Fig. 3 Scanning electron microscopy images with frequency of "fiber diameter distribution" and "porous area fraction" value (diagrams below the corresponding SEM image) of electrospun membranes immobilized with different coatings of MXenes: PCL-MX1 **a**, PCL-MX2 **b,** and PCL-MX3 **c** and after the oxygen plasma treatment: PCL-MX1-PL **d**, PCL-MX2-PL **e,** and PCL-MX3-PL **f**. The magnification for all images is × 5000 (scale bar = 10 µm). Insertions on **a** and **d**—HRTEM demonstrated MXene deposition (blue arrow) on PCL fiber (scale bar = 10 nm)

atomic percentage concentration of Ti when compared to the non-treated group.

The utilization of 3D imaging aided in the interpretation of scaffold morphology and facilitated a better understanding of the interaction between MXenes and fibers (see Fig. 5). The data obtained indicate that MXenes have no significant influence on the roughness and closely resemble the form of the fiber membrane structure (*Ra* and *Rz* data in Fig. 5). Furthermore, the 3D visualization suggests the presence of layered MXene films on the surface after the second and third treatments.

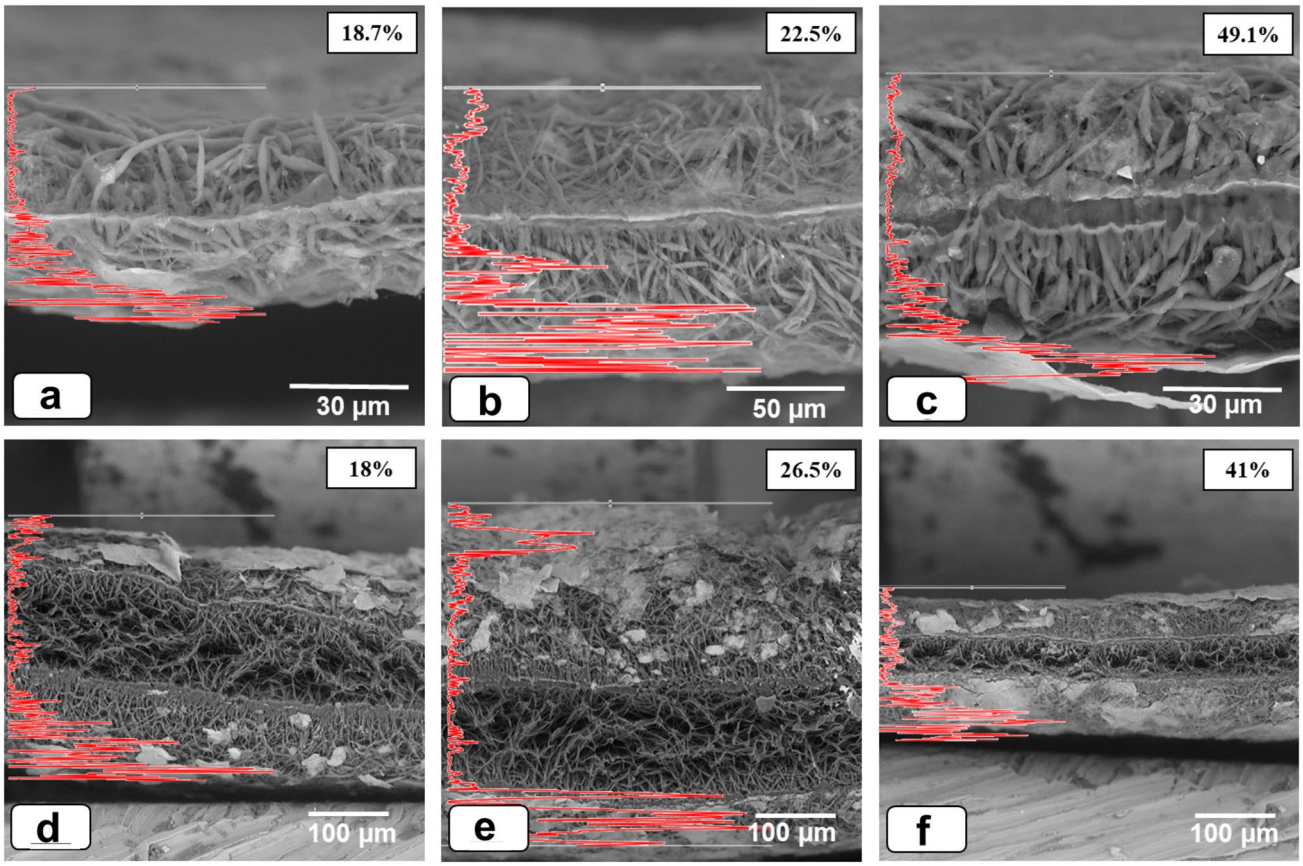

Fig. 4 Scanning electron microscopy images of membranes' cross-section with cross-sectional EDX line scan (red diagrams) and EDS atomic % of Ti. Figure demonstrating membranes with different coatings of MXene: PCL-MX1 **a**, PCL-MX2 **b,** and PCL-MX3 **c** and after oxygen plasma treatment: PCL-MX1-PL **d**, PCL-MX2-PL **e,** and PCL-MX3-PL **f**

4.2 Chemical patterns of PCL-MXene membranes

The FTIR-ATR spectrum of PCL-MX-PL (see Fig. 6a) exhibits contributions from both the PCL and MXene phases. The signals observed at 2940–2860 cm^{-1} correspond to the asymmetric and symmetric axial deformations (ν(C–H)) of the CH_2 group. The most prominent peak observed is associated with the stretching of the C=O bond at 1722–cm^{-1}. According to the literature [46], the band observed at 1293 cm^{-1} can be attributed to the vibrations of the ν(C–O) and ν(C–C) bonds in the crystalline form of the PCL chain. The broad but weak peak observed at 960 cm^{-1} in the PCL samples splits into two distinct peaks as the crystallinity increases: one intense and narrow peak at 960 cm^{-1}, and another at 940 cm^{-1}, which can be assigned to the ester bond (δ(C–O–C)). Similarly, the peak observed at 740–730 cm^{-1} (attributed to ρ(CH_2)) is indicative of the polymer crystallinity, as it splits into two separate peaks (732 cm^{-1} and 711 cm^{-1}) in highly crystalline PCL samples. The presence of MXene on the surface of the samples is confirmed by the signals observed at 665 cm^{-1} (ν(Ti–O) bond deformation), 1395 cm^{-1} (δ(O–H) bending vibration of terminal groups in MXene or chemisorbed water), and 1096 cm^{-1} (deformation vibration of ν(C–F), related to MXene surface terminations).

All the investigated free-standing membranes exhibited characteristic vibrations, represented by peaks at 205, 255, 286, 405, 550, 622, and 725 cm^{-1}. However, slight variations in peak intensities were observed (see Fig. 6b). The out-of-plane Raman (A1g) modes at 205 cm^{-1} and the in-plane E1g modes at 255, 286, and 405 cm^{-1} indicate vibrations associated with surface groups of titanium. The E1g and A1g peaks at 550/622 cm^{-1} and 724 cm^{-1}, respectively, correspond to carbon vibrations. The Raman peaks in the MXene phase can be attributed to Ti–C, C–C, and C–O bonds. The broadening and merging of lines in the spectra suggest the exfoliation and delamination of the Ti_3AlC_2 precursor. The absence of sharp signals at 135 cm^{-1} indicates complete etching of Ti_3AlC_2 from the MXene. The presence of a hump at 400 cm^{-1} indicates the heterogeneous nature of terminal groups, consisting of –O and –OH ending groups [47].

The Raman spectra do not exhibit signals from the PL jet. This can be attributed to the excellent electrical conductivity of MXene flakes, which leads to shallow penetration of

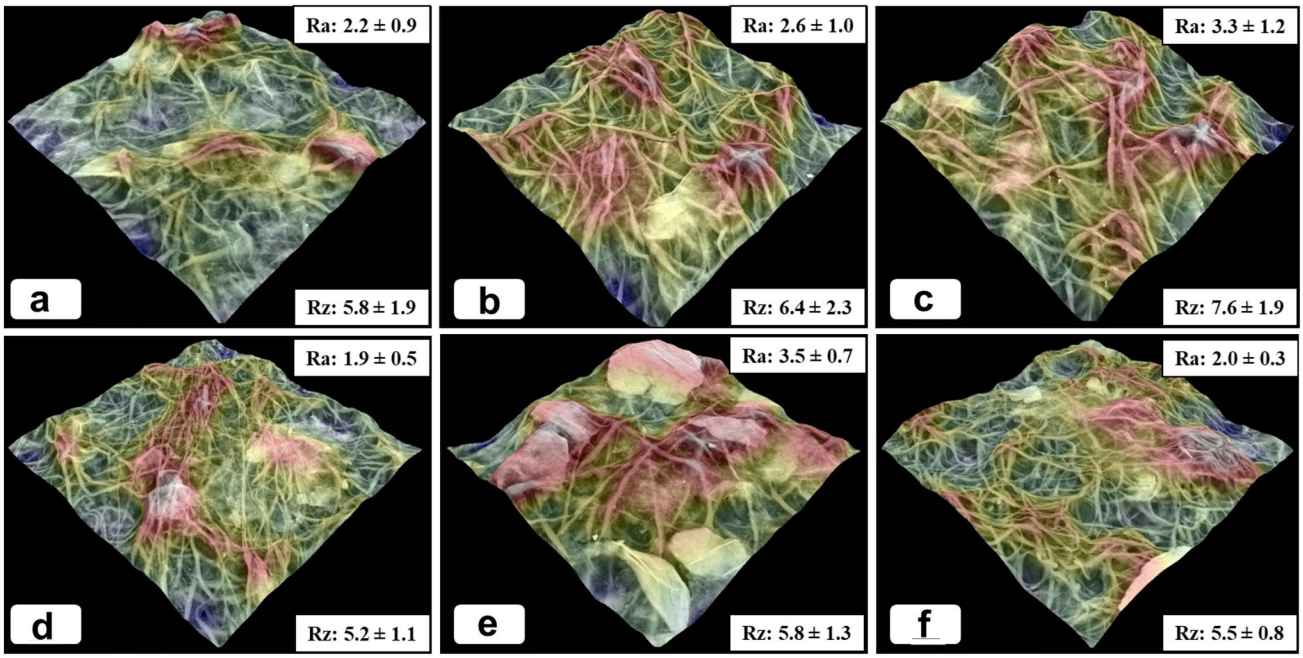

Fig. 5 Three-dimensional reconstruction of surface morphology of electrospun membranes immobilized with different coatings of MXene: PCL-MX1 **a**, PCL-MX2 **b,** and PCL-MX3 **c** and immobilized with different coatings of MXene after oxygen plasma treatment: PCL-MX1-PL **d**, PCL-MX2-PL **e,** and PCL-MX3-PL **f**. In the insertions—the roughness reconstruction of the membrane texture (*Ra*, μm and *Rz*, μm)

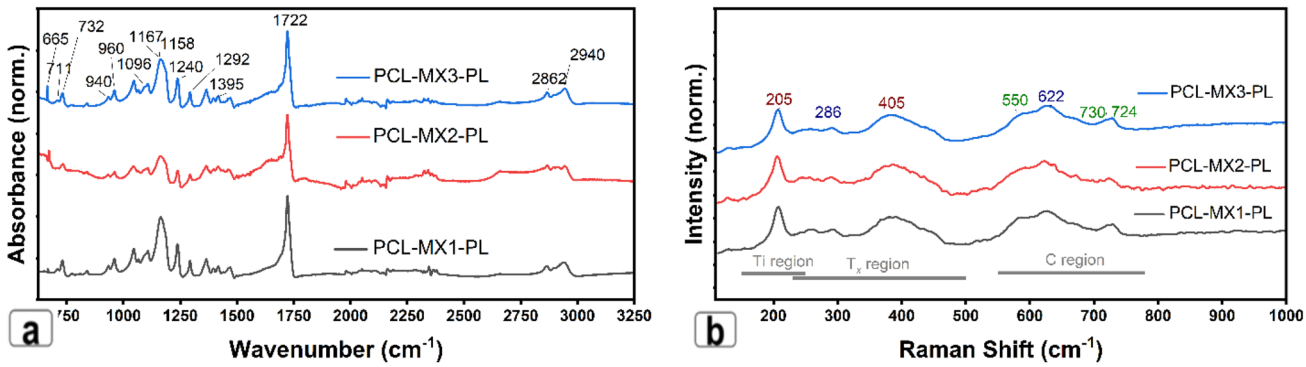

Fig. 6 IR-ATR **a** and Raman spectra **b** of PCL-MX-PL membranes

the laser beam into the membrane material. This shallow penetration is a result of the electromagnetic interaction between the excitation light and the conductive matter. Consequently, the collected spectra provide information about the outermost surface of the stacked MXenes, confirming the complete surface coverage of the PL membranes with MXene flakes.

4.3 Surface wettability

The surface wettability of the PCL membranes was evaluated using sessile drop analysis. Contact angles below 90° indicated hydrophilic surfaces, while angles above 90° indicated low wettability or hydrophobic surfaces [48]. Surface wettability is crucial for determining the functionality of membranes for tissue engineering and regenerative medicine: More hydrophilic surfaces facilitate protein adsorption that leads cell adhesion and proliferation [49]. Temporary surface wettability modification can be achieved through chemical coating and plasma treatment. Oxygen plasma treatment offers a non-permanent modification effect as the treated surfaces return to their original characteristics [50], allowing the membranes to serve different purposes over time.

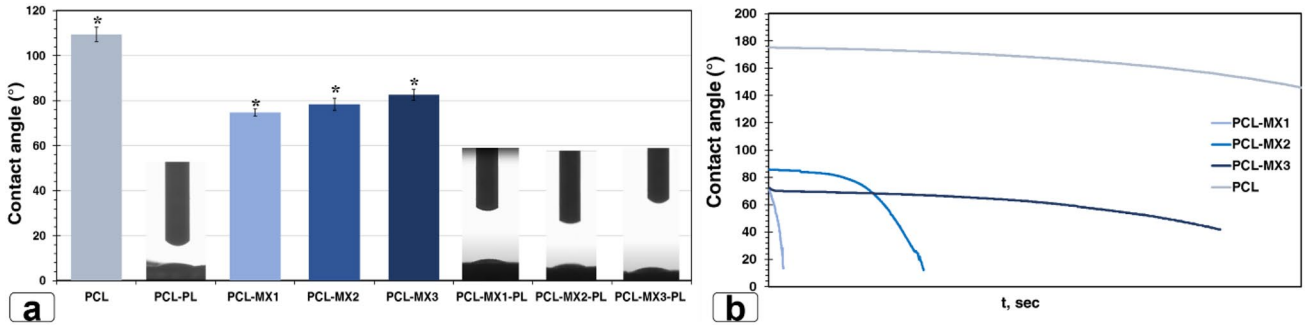

Fig. 7 Diagrams of static **a** and dynamic **b** contact angle measurements. Asterisks denote significant differences between free PCL and PCL-MX scaffolds at $p \leq 0.05$

The PCL membrane exhibited hydrophobic behavior, as indicated by the obtuse contact angle of water droplets ($109.5° \pm 3.5°$) (Fig. 7a). Plasma treatment significantly altered the surface properties of the PCL membrane, rendering it highly hydrophilic with a contact angle of 0°. This fact allows to facilitate MXenes deposition on hydrophilic PCL membrane. Previously, we used chemical treatment of hydrophobic PCL membrane using alkali or acidic solution, but with less significant effect on PCL mats contact angle [40]. Additionally, plasma treatment is a safer method due to the lack of toxic residuals after pretreatment that should affect cell growth and proliferation. The incorporation of MXenes into the membrane slightly increased the static contact angle to $82.7° \pm 2.5°$ with no significant difference between deposition times. Post-treatment of PCL-MXenes membranes with oxygen plasma turns the contact angle to 0^0 that should be due to the introduction of hydrophilic groups (O^- and OH^-) over the surface. Other studies have shown that plasma treatment generates oxygen-containing functional groups, leading to a chemical change in the surface layer and the transformation of hydrophobic surfaces into hydrophilic ones [50].

To further investigate surface wettability, dynamic contact angles were measured for PCL and PCL-MX samples (Fig. 7b). The PCL-MX-PL group was excluded from this investigation due to superhydrofillic nature of their surface. The water absorption rate decreased with increasing MXenes content, consistent with the limited water absorption capacity of PCL membranes. The amount of MXenes coating influenced the speed of surface absorption. The water absorption rate decreased by 25.5 times for PCL-MX2 samples and 104 times for PCL-MX3 compared to PCL-MX1. The tunable effect of MXenes treatment allowed for modification of the wettability and water absorption capacity of the PCL scaffolds. This fact should be described by faster introduction of hydrophilic groups, such as O^- and OH^-, during plasma treatment on MXene surface compared to pure PCL membranes.

4.4 Electrical conductivity

PCL and PCL-PL samples showed resistance above 40 MOhm (measurement limit of the instrument). Resistance was measurable for samples with MXene, and the mean values ranged from 0.74 to 26.78 kOhm. Values of these measurements are shown in Fig. 8 (left). The conductivity was recalculated, fitting the range of 5.22–326.33 mS/m (Fig. 8 right).

The high electrical conductivity of MXene materials makes them particularly suitable for cardiac tissue

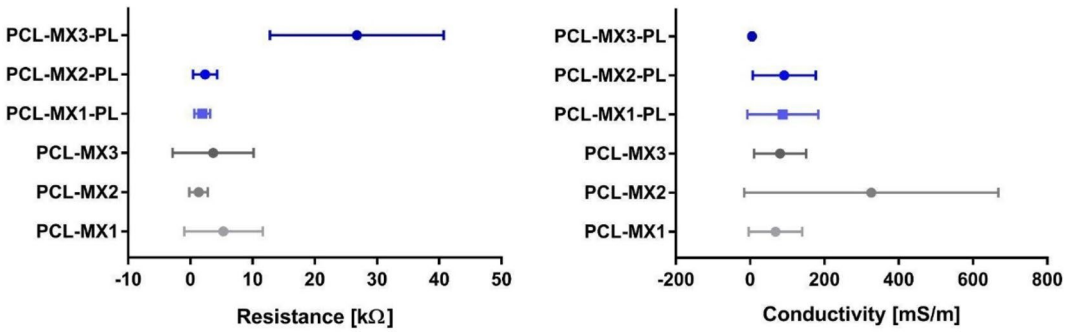

Fig. 8 Measured resistance and recalculated conductivity of MXene-coated PCL membranes

engineering [24, 51]. Material conductivity is essential for cardiac tissue repair, since the conductivity of normal myocardium is about 1 mS/m [52], and non-conductive materials interfere with the transmission of electrical signals necessary for coordinated heart cell contraction and heartbeat. Incorporating MXene materials as a surface layer over a polycaprolactone dielectric can potentially enhance the electrical conductivity of the composite, thereby facilitating the electrical communication between cells in the cardiac tissue.

Several studies have highlighted the importance of electrical conductivity in cardiac tissue engineering. For example, MXene materials have been shown to exhibit exceptional electrical conductivity, which can improve the electrical coupling between cells in cardiac tissue constructs, leading to enhanced tissue function [53]. In addition, the use of MXene as a conductive layer in cardiac tissue engineering scaffolds has been reported to promote the proliferation and differentiation of cardiac cells, leading to improved tissue regeneration and functional outcomes [54].

One of the primary ways in which the electrical conductivity of PCL-MXene scaffolds impacts tissue regeneration is by promoting enhanced electrical communication between cells. In cardiac tissue engineering, for example, efficient transmission of electrical signals is critical for synchronized cell contraction and overall heart function [55]. The native electrical conductivity of myocardium, approximately 1 mS/m, is essential for this coordination. By incorporating MXene materials with high electrical conductivity as a surface layer over a polycaprolactone dielectric, we aim to bridge this gap and facilitate improved electrical coupling between cells. In our research, we demonstrated advanced conductivity required for cardiac application. Recent research [56] demonstrated MXene conductivity up to 2.80 S/cm, but scaffold was made by electric field-driven jet 3D printing and electrostatic self-assembly with aligned orientation that is favorable for electron transport. In contrast with this research, our scaffold has some limitations such as randomly oriented fibers and high porosity that limited conductivity. While the incorporation of conductive scaffolds offers significant benefits, several challenges must be addressed. One crucial aspect is the control of topography and the provision of appropriate biochemical cues [57, 58]. The physical structure and surface properties of scaffolds greatly influence cell behavior, including adhesion, proliferation, and differentiation. Combining electrical conductivity with carefully designed topographical features and biochemical cues is essential to guide cell responses and promote tissue regeneration effectively. Achieving this balance is a complex task that requires thorough optimization. Another critical consideration is the interconnected porosity of scaffolds [59]. Adequate porosity is essential to ensure proper mass transport, including the exchange of nutrients and waste products. In conductive scaffolds, maintaining this interconnected porosity while preserving electrical conductivity can be challenging. Careful scaffold design, which allows for both efficient electrical signaling and effective mass transport, is essential for successful tissue regeneration.

It is important to note that the significance of electrical conductivity in tissue engineering extends beyond cardiac applications. The approach of using MXene materials as conductive surface layers can be adapted for neural tissue regeneration and neural conduits engineering. Neurons rely on electrical signaling for communication, and conductive scaffolds can enhance neural tissue function by facilitating these signals. The principles discussed here are applicable to various tissue engineering contexts where electrical communication is a critical factor in tissue development and repair.

4.5 Membrane degradation

Polycaprolactone is a biodegradable synthetic polymer with a slow degradation rate due to its semi-crystalline and hydrophobic nature, which limits its applications in tissue engineering [60]. However, the electrospinning method increases the surface area-to-volume ratio and reduces crystallinity, thereby accelerating the degradation rate [61]. In the static mode of degradation testing, we observed no significant mass loss before week 3, but by week 4, there was a substantial reduction in mass. Notably, there was a marked difference in the degradation behavior between pure PCL and the PCL-MXene composite. Applying one or two coatings of MXenes to the composite significantly protected the material from degradation. Conversely, plasma treatment of the PCL-MXene composite notably increased mass loss in PBS. Our hypothesis is that plasma treatment greatly enhanced the hydrophobic nature of PCL, leading to the polymer's hydralization. The thin layer of MXene (1 and 2 coatings) effectively shielded PCL fibers from direct water contact, thereby reducing the degradation rate. In the case of multiple coatings (PCL-MX3), they led to the formation of multilayered structures, which exfoliated upon contact with water, increasing their interaction with PCL fibers. As a result, PCL, PCL-MX3, and PCL-MX2-PL experienced a mass loss ranging from 29 to 33% of their initial weight, while PCL-MX1 and PCL-MX2 exhibited significantly lower mass loss, around 5% from their initial weight (Fig. 9a).

Dynamic degradation experiment demonstrated that continuous PBS flow significantly increases degradation of both pure PCL electrospun mats and PCL-MXene composite membrane. The degradation started from week 2 and the most dramatic weight loss was observed for PCL-MX2-PL and PCL-MX3-PL membranes (up to 65.36%), which proves our hypothesis about the influence of oxygen plasma. PCL-MX1 and PCL-MX3 membranes lost up to 28% of initial weight (Fig. 9b).

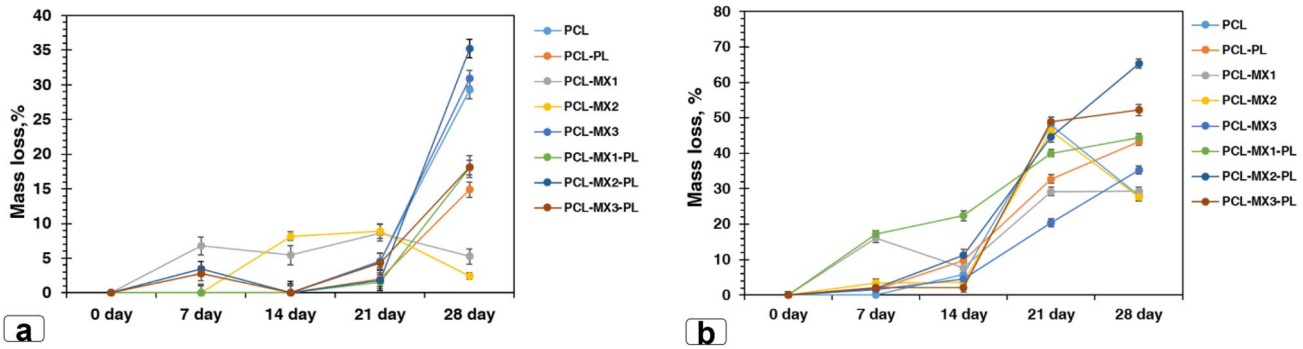

Fig. 9 Dynamic of PCL and PCL-MX material degradation in static **a** and dynamic **b** conditions

These findings collectively highlight the intricate interplay among material composition, treatment methods, and degradation behaviors—critical factors to consider in the design of biomaterials for tissue engineering applications. Importantly, it should be noted that the material's properties undergo significant changes when PCL is loaded with multiple layers of MXenes. This study successfully validated our hypothesis [33], demonstrating that one or two layers of MXene are sufficient to create a highly conductive and biocompatible scaffold. Moreover, additional treatments, such as oxygen plasma exposure, can substantially impact degradation rates, an aspect that warrants careful consideration for *in vivo* and clinical applications.

Furthermore, it is essential to assess the material's degradation behavior following various fabrication methods, such as electrospinning, 3D printing, and others, as these processes can significantly influence the rate of degradation.

4.6 Biocompatibility

Numerous studies have demonstrated sufficient cell adhesion and proliferation on PCL nanofibrous scaffolds, particularly after modifications that increase surface wettability [43]. Our previous results have shown that alkali and acidic pretreatment of electrospun PCL membranes decrease the contact angle and facilitate the deposition of MXenes, resulting in a sufficient rate of cell adhesion and proliferation [42]. However, due to the biodegradation of PCL membranes, the release of chemicals used for pretreatment (such as H_2SO_4 and NaOH) is anticipated to have adverse effects on tissue remodeling. Some research has demonstrated the direct mixture of $T_3C_2T_x$ MXenes in collagen with gelatin as a dispersion agent for the development of an electroconductive scaffold. However, the high concentration of MXene (ranging from 15 to 75% w/w) makes this scaffold has limited biocompatibility and increases the risk of MXene release [25]. Another study used MXene Ti_2C to incorporate into a cryogel, resulting in a conductive cardiac patch that promoted functional maturation of cardiomyocytes and enhanced the repair of myocardial infarction [62]. Although 3D printing has also been used to produce cardiac tissue substitutes with MXene deposition, these grafts did not demonstrate the electroconductivity of the native human heart, despite exhibiting an appropriate cell response [51]. Therefore, electrospinning should be the method of choice for fast and reproducible manufacturing of cardiac tissue patches from PCL, followed by MXene deposition. Using a fast, low-cost, and safe method of wettability control (oxygen plasma), we successfully produced highly conductive and biocompatible patches.

We demonstrated the appropriate fibroblast cell adhesion and proliferation in all experimental groups, including the PCL non-treated control and all versions with MXene deposition (Supplement, Fig. S4). On day 7, we observed a uniform and aligned distribution of fibroblasts (Fig. 10) over the surface of both free and MXene-loaded PCL membranes. At high magnification, the formation of tight cell–cell contacts resembling symplasts was observed. We hypothesized that the application of the PCL-MXene membrane to damaged heart tissue would improve the conduction of electrical signals from healthy tissue to ischemic tissue through MXene, which, in turn, would improve the contractile function of the heart.

Furthermore, electroconductive PCL-MXene electrospun fibers could be used for myocardial tissue engineering due to the remarkable properties of MXenes. They demonstrate the ability to reduce the recruitment of selected immune cells, such as human T-lymphocytes, promote immunosuppressive regulatory T cells, and limit secondary injury to the heart [63]. Additionally, certain MXenes (such as Ta_4C_3) can inhibit undesired cellular immune responses during the healing process by regulating surface co-activator and co-inhibitor molecules [64]. Moreover, $Ti_3C_2T_x$ MXenes have shown the ability to promote iPSC-derived cardiomyocyte maturation by controlling cx43 expression [65].

To summarize the biocompatibility section, we can confirm the safety of PCL-MX and PCL-MX-PL membranes with the ability to support cell adhesion and proliferation.

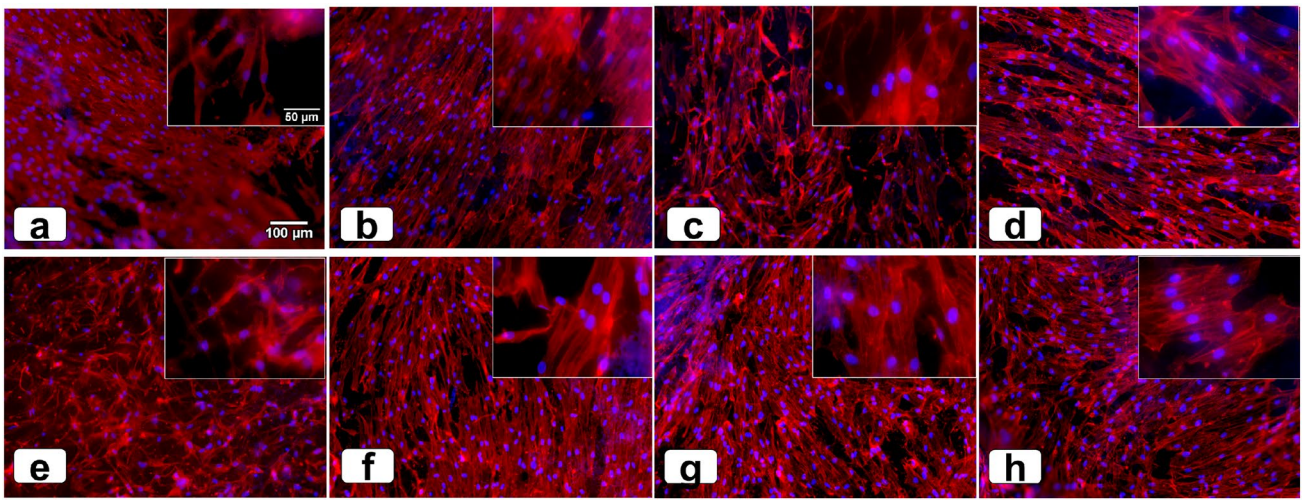

Fig. 10 Fluorescent images of nuclei (blue) and cytoskeleton staining (red) on the 7th day of dermal fibroblasts on PCL membranes with various numbers of deposited layers, where PCL **a**, PCL-MX1 **b**, PCL-MX2 **c**, PCL-MX3 **d**, PCL-PL **e**, PCL-MX1-PL **f**, PCL-MX2-PL **g,** and PCL-MX3-PL **h**. The magnification of the main images is × 100 (scale bar = 100 µm),and on the insets—× 400 (scale bar = 50 µm)

4.7 Antibacterial properties

Several reports demonstrate the antibacterial properties of different MXenes, including Ti_3C_2, both in suspension and after deposition on surfaces [66–68]. However, our previous study did not find strong antibacterial properties, but it did observe some bacteriostatic activity in the short-term period after contact of bacteria with MXenes [40, 41]. In this study, we provide two different measurements of the resazurin reduction assay: one directly on the membrane and another after removing the bacteria using sonication. We conducted the second measurement to mitigate the risk of false-positive results, considering the potential autoreduction ability of MXenes. Current results indicate that there is an increase in bacteria growth on the membrane with no significant effect of different MXene depositions (Fig. 11). Furthermore, the resazurin reduction assay conducted with bacteria that were removed from the PCL-MX membrane also did not show the antibacterial activity of the novel material (see Supplement, Fig. S5).

Scanning electron microscopy of PCL and PCL-MXene membranes revealed significant bacterial colonization on the surface of the materials. Both *St. aureus* (Fig. 12) and *E. coli* (Supplement, Fig. 6) were observed to occupy the superficial fibers and penetrate inside the pores of the membranes. Importantly, it was noted that bacteria exhibited a preference for attaching to MXene flakes compared to PCL fibers. The presence of terminal groups on Ti_3C_2 MXenes is believed to facilitate non-specific bacterial adhesion, particularly after oxygen plasma treatment, which promotes the formation of additional O^- and OH^- groups. In summary, the immobilized MXenes did not exhibit antibacterial activities, but rather facilitated their attachment. There are several ways that could improve the antibacterial potential of PCL-MX scaffolds. MXene with large surface area and active termination [69] could serve as a platform for the drug

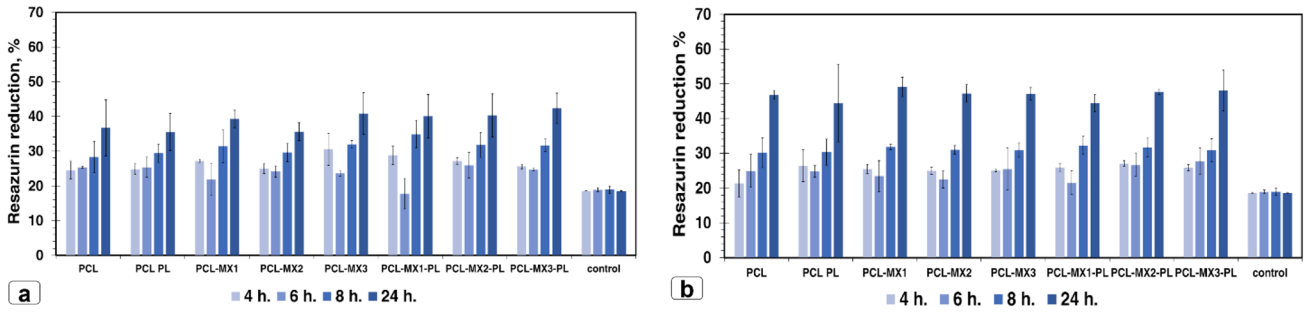

Fig. 11 Antibacterial properties against **a** *St. aureus* and **b** *E. coli* were determined by resazurin reduction assay of membranes covered with bacteria and put into nutrient broth with resazurin

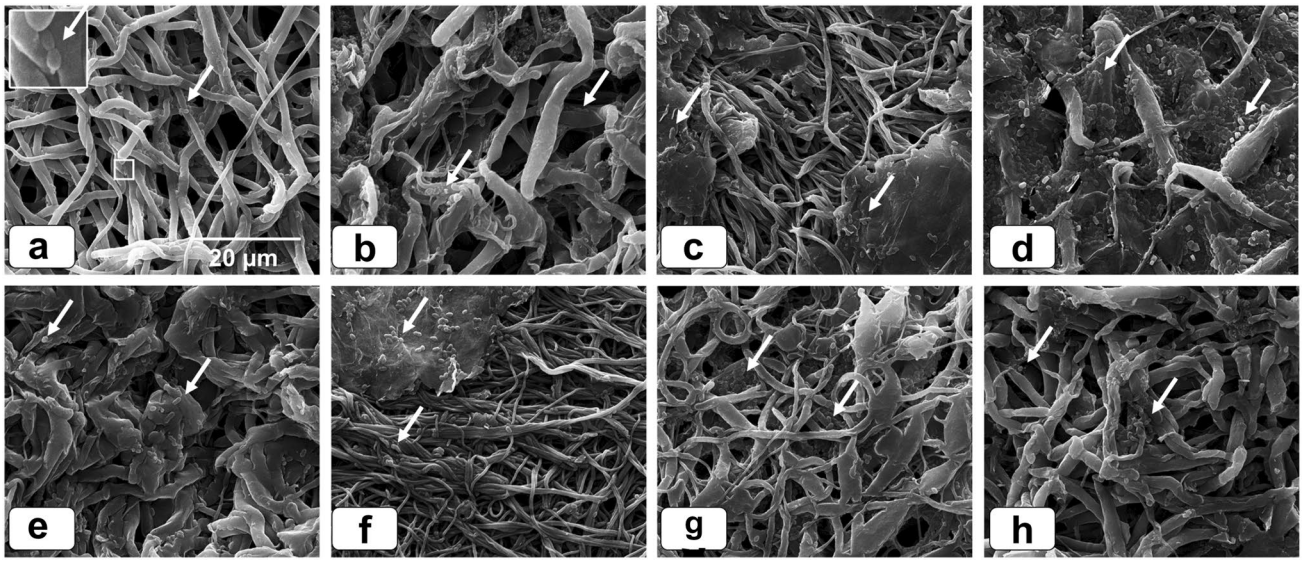

Fig. 12 Scanning electron microscopy imaging of PCL membranes with *St. aureus* after 24 h of incubation. PCL **a**, PCL-MX1 **b**, PCL-MX2 **c**, PCL-MX3 **d**, PCL-PL **e**, PCL-MX1-PL **f**, PCL-MX2-PL **g**, and PCL-MX3-PL **h**. Magnification—5000. Arrows demonstrate single bacteria cells

delivery concept and binding with an antibacterial agent should prevent possible infection after operative procedure. The high photo-thermal conversion ability of MXenes in the near-infrared region actively exploits in anticancer and antibacterial research that also could be used as a guided antibacterial strategy in case of infection. But both strategies require detailed research and validation.

5 Conclusion

In this research, we have developed a new method for depositing $Ti_3C_2T_x$ MXenes onto hydrophobic electrospun PCL membranes using oxygen plasma treatment. This innovative approach has demonstrated a positive impact on fiber size, increased the porous structure and significantly reducing the contact angle of the PCL membrane and facilitating deep impregnation of MXene into the material. Importantly, this deposition technology has not affected the chemical parameters of the PCL membrane and is not expected to cause any toxic effects upon degradation. The resulting PCL-MXene composite membrane exhibits the desired conductive properties necessary for cardiac tissue regeneration, with no significant differences observed between the various numbers of MXene depositions. Furthermore, the additional treatment of the PCL-MXene membrane with oxygen plasma introduces hydrophilic groups (O^- and OH^-) that greatly reduce the contact angle, which is crucial for cell attachment. All types of PCL-MXene membranes demonstrate high biocompatibility, as evidenced by the formation of cell symplasts on day 7 after seeding. However, it is essential to note that these membranes did not exhibit antibacterial properties. Overall, the incorporation of MXenes into biodegradable PCL membranes shows promise in conferring electroconductivity and enhancing cellular response in tissue-engineered cardiac patches. These novel patches hold tremendous potential for providing mechanical support to damaged heart tissue and enabling electrical signal transmission, thereby mimicking the crucial electroconductivity required for normal cardiac function. Considering the lack of difference in conductivity and cell proliferation, only one set of MXene deposition using a novel technique is sufficient for the development of cardiac tissue substitutes. After a detailed investigation of scaffold-to-cell interplay, including electrical stimulation, novel technology has the potential for clinical application not only for cardiac regeneration, but also as neural and muscular tissue substitutes.

Supplementary Information The online version contains supplementary material available at https://doi.org/10.1007/s41127-023-00071-5.

Acknowledgements This research was supported by Horizon Europe MSCA-2021-SE-01 project MX-MAP (#101086184) and H2020-MSCA-RISE-2019 SALSETH (#872370) and received support from the Ministry of Education and Science of Ukraine (0122U000784).

Author contributions K.D. - Conceptualisation, membrane preparation, cell culture, wrote the manuscript; Y. H. - contact angle, 3D visualization; W. S. - Raman, 3D visualization; V. K. - bacteriology experiment; B. Petrovic - conductivity measurements, SEM; A. R. - SEM of bacteria, 3D visualization; A. Stolarczyk - FTIR; N.Waloszczyk - Raman; I. Yanko - SEM of bacteria, figure preparation; K. Jekabsons - cell fluorescent microscopy; M. Čaplovičová - HRTEM; A.D.P. - HRTEM and manuscript writing; V. Z. - MXene preparation; O. Gogotsi -MAX-phase synthesis; I.Roslyk - MXene synthesis and

delamination; I. Baginskiy - membrane impregnation of MXene; M. Radovic - electroconductivity measurement; S. Kojic - electroconductivity description; U. R. -conceptualization of biological experiment, manuscript writing; M. P. - supervision. manuscript writing and correction. All authors reviewed the manuscript.

Data availability The raw/processed data required to reproduce these findings cannot be shared at this time as the data also form part of an ongoing study. The raw data are available on request.

Declarations

Conflict of interest Authors declare no conflicting interest.

References

1. Mortality and global health estimates (2022) [Online]. Available: https://www.who.int/news/item/09-12-2020-who-reveals-leading-causes-of-death-and-disability-worldwide-2000-2019.
2. European Cardiovascular Disease Statistics (2017) edition
3. Baei P, Hosseini M, Baharvand H, Pahlavan S (2020) Electrically conductive materials for in vitro cardiac microtissue engineering. J Biomed Mater Res Part A 108(5):1203–1213. https://doi.org/10.1002/JBM.A.36894
4. Alegret N, Dominguez-Alfaro A, Mecerreyes D (2019) 3D scaffolds based on conductive polymers for biomedical applications. Biomacromol 20(1):73–89. https://doi.org/10.1021/ACS.BIOMAC.8B01382/ASSET/IMAGES/LARGE/BM-2018-013823_0013.JPEG
5. Yanamandala M et al (2017) Overcoming the roadblocks to cardiac cell therapy using tissue engineering. J Am Coll Cardiol 70(6):766–775. https://doi.org/10.1016/J.JACC.2017.06.012
6. Weinberger F, Mannhardt I, Eschenhagen T (2017) Engineering cardiac muscle tissue: a maturating field of research. Circ Res 120(9):1487–1500. https://doi.org/10.1161/CIRCRESAHA.117.310738
7. Scott L, Jurewicz I, Jeevaratnam K, Lewis R (2021) Carbon nanotube-based scaffolds for cardiac tissue engineering—Systematic review and narrative synthesis. Bioengineering. https://doi.org/10.3390/BIOENGINEERING8060080
8. You JO, Rafat M, Ye GJC, Auguste DT (2011) Nanoengineering the heart: conductive scaffolds enhance connexin 43 expression. Nano Lett 11(9):3643–3648. https://doi.org/10.1021/NL201514A/SUPPL_FILE/NL201514A_SI_002.AVI
9. Orza A et al (2011) Electrically conductive gold-coated collagen nanofibers for placental-derived mesenchymal stem cells enhanced differentiation and proliferation. ACS Nano 5(6):4490–4503. https://doi.org/10.1021/NN1035312/SUPPL_FILE/NN1035312_SI_001.PDF
10. Ravichandran R, Sridhar R, Venugopal JR, Sundarrajan S, Mukherjee S, Ramakrishna S (2014) Gold nanoparticle loaded hybrid nanofibers for cardiogenic differentiation of stem cells for infarcted myocardium regeneration. Macromol Biosci 14(4):515–525. https://doi.org/10.1002/MABI.201300407
11. Baei P, Jalili-Firoozinezhad S, Rajabi-Zeleti S, Tafazzoli-Shadpour M, Baharvand H, Aghdami N (2016) Electrically conductive gold nanoparticle-chitosan thermosensitive hydrogels for cardiac tissue engineering. Mater Sci Eng C Mater Biol Appl 63:131–141. https://doi.org/10.1016/J.MSEC.2016.02.056
12. Sherrell PC et al (2017) Rational design of a conductive collagen heart patch. Macromol Biosci 17(7):1600446. https://doi.org/10.1002/MABI.201600446
13. Wu Y, Wang L, Guo B, Ma PX (2017) Interwoven aligned conductive nanofiber yarn/hydrogel composite scaffolds for engineered 3d cardiac anisotropy. ACS Nano 11(6):5646–5659. https://doi.org/10.1021/ACSNANO.7B01062/SUPPL_FILE/NN7B01062_SI_008.AVI
14. Izadifar M, Chapman D, Babyn P, Chen X, Kelly ME (2018) UV-assisted 3d bioprinting of nanoreinforced hybrid cardiac patch for myocardial tissue engineering. Tissue Eng Part C Methods 24(2):74–88. https://doi.org/10.1089/TEN.TEC.2017.0346
15. Ahadian S et al (2017) Moldable elastomeric polyester-carbon nanotube scaffolds for cardiac tissue engineering. Acta Biomater 52:81–91. https://doi.org/10.1016/J.ACTBIO.2016.12.009
16. Hitscherich P et al (2018) Electroactive graphene composite scaffolds for cardiac tissue engineering. J Biomed Mater Res A 106(11):2923–2933. https://doi.org/10.1002/JBM.A.36481
17. Bao R, Tan B, Liang S, Zhang N, Wang W, Liu W (2017) A π-π conjugation-containing soft and conductive injectable polymer hydrogel highly efficiently rebuilds cardiac function after myocardial infarction. Biomaterial 122:63–71. https://doi.org/10.1016/J.BIOMATERIALS.2017.01.012
18. Smith AST et al (2017) Micro- and nano-patterned conductive graphene–PEG hybrid scaffolds for cardiac tissue engineering. Chem Commun 53(53):7412–7415. https://doi.org/10.1039/C7CC01988B
19. Liu H et al (2023) An electroconductive hydrogel scaffold with injectability and biodegradability to manipulate neural stem cells for enhancing spinal cord injury repair. Biomacromolecule 24(1):86–97. https://doi.org/10.1021/acs.biomac.2c00920
20. Furlani F et al (2023) Electroconductive scaffolds based on gelatin and PEDOT:PSS for cardiac regeneration. Int J Biol Macromol 224:266–280. https://doi.org/10.1016/j.ijbiomac.2022.10.122
21. Srinivasan SY et al (2023) Conductive bacterial nanocellulose-polypyrrole patches promote cardiomyocyte differentiation. ACS Appl Bio Mater. https://doi.org/10.1021/acsabm.3c00303
22. Ghosh S, Dhiman M, Gupta S, Roy P, Lahiri D (2023) Electroconductive chitosan/graphene bio-nanocomposite scaffold for tissue engineering of the central nervous system. Biomaterial. https://doi.org/10.1016/j.bioadv.2023.213596
23. Nekounam H et al (2021) Electroconductive scaffolds for tissue regeneration: Current opportunities, pitfalls, and potential solutions. Mater Res Bull. https://doi.org/10.1016/j.materresbull.2020.111083
24. Gogotsi Y, Anasori B (2019) The Rise of MXenes. ACS Nano 13(8):8491–8494. https://doi.org/10.1021/acsnano.9b06394
25. Gokce C, Gurcan C, Delogu LG, Yilmazer A (2022) 2D materials for cardiac tissue repair and regeneration. Front Cardiovasc Med. https://doi.org/10.3389/FCVM.2022.802551
26. Gazzi A et al (2019) Photodynamic therapy based on graphene and MXene in cancer theranostics. Front Bioeng Biotechnol. https://doi.org/10.3389/FBIOE.2019.00295/BIBTEX
27. Kyrylenko S et al (2022) MXene-assisted ablation of cells with a pulsed near-infrared laser. ACS Appl Mater Interfaces 14(25):28683–28696. https://doi.org/10.1021/ACSAMI.2C08678/ASSET/IMAGES/LARGE/AM2C08678_0011.JPEG
28. Fusco L et al (2023) V_4C_3 MXene immune profiling and modulation of t cell-dendritic cell function and interaction. Small Methods. https://doi.org/10.1002/smtd.202300197
29. Fusco L et al (2022) Immune profiling and multiplexed label-free detection of 2d mxenes by mass cytometry and high-dimensional imaging. Adv Mater. https://doi.org/10.1002/adma.202205154
30. Peng G, Keshavan S, Delogu L, Shin Y, Casiraghi C, Fadeel B (2022) Two-dimensional transition metal dichalcogenides trigger trained immunity in human macrophages through epigenetic and metabolic pathways. Small 18:20. https://doi.org/10.1002/smll.202107816

31. Driscoll N et al (2021) MXene-infused bioelectronic interfaces for multiscale electrophysiology and stimulation. Sci Transl Med. https://doi.org/10.1126/SCITRANSLMED.ABF8629/SUPPL_FILE/SCITRANSLMED.ABF8629_DATA_FILE_S1.ZIP
32. Wang Y et al (2021) $Ti_3C_2T_x$MXene flakes for optical control of neuronal electrical activity. ACS Nano 15(9):14662–14671. https://doi.org/10.1021/ACSNANO.1C04431/SUPPL_FILE/NN1C04431_SI_004.PDF
33. Li Y et al (2023) Toward Smart Sensing by MXene. Small. https://doi.org/10.1002/smll.202206126
34. Lai QT, Zhao XH, Sun QJ, Tang Z, Tang XG, Roy VAL (2023) Emerging MXene-based flexible tactile sensors for health monitoring and haptic perception. Small. https://doi.org/10.1002/smll.202300283
35. Manisekaran R, Chettiar ADR, Kandasamy G, GarciaContreras R, AcostaTorres LS (2023) State of the art: MXene structures in nano oncology. Biomater Adv 147:213354. https://doi.org/10.1016/j.bioadv.2023.213354
36. Solangi NH, Mazari SA, Mubarak NM, Karri RR, Rajamohan N, Vo DVN (2023) Recent trends in Mxene based material for biomedical applications. Environ Res 222:115337. https://doi.org/10.1016/j.envres.2023.115337
37. Schmitt PR, Dwyer KD, Coulombe KLK (2022) Current applications of polycaprolactone as a scaffold material for heart regeneration. ACS Appl Bio Mater 5(6):2461–2480. https://doi.org/10.1021/acsabm.2c00174
38. Park D, Lee SJ, Choi DK, Park JW (2023) Therapeutic agent-loaded fibrous scaffolds for biomedical applications. Pharmaceutics. https://doi.org/10.3390/pharmaceutics15051522
39. Kołtunowicz TN et al (2021) Investigation of AC electrical properties of mxene-pcl nanocomposites for application in small and medium power generation. Energies 14(21):7123. https://doi.org/10.3390/en14217123
40. Diedkova K et al. (2022) The Multistep Process of Coating PCL Membranes with MXene Solution pp. NRA17–1-NRA17–4: https://doi.org/10.1109/NAP55339.2022.9934231
41. Kyrylenko S et al. (2020) Bio-Functionalization of Electrospun Polymeric Nanofibers by Ti_3CT_x MXene Proc 2020 IEEE 10th Int. Conf. Nanomaterials Appl. Prop. N. 2020: https://doi.org/10.1109/NAP51477.2020.9309612
42. Diedkova K et al (2022) Polycaprolactone-MXene nanofibrous scaffolds for tissue engineering. ACS Appl Mater Interfaces. https://doi.org/10.1021/acsami.2c22780
43. Seddighian A, Ganji F, Baghaban-Eslaminejad M, Bagheri F (2021) Electrospun PCL scaffold modified with chitosan nanoparticles for enhanced bone regeneration. Prog Biomater 10(1):65–76. https://doi.org/10.1007/s40204-021-00153-8
44. Zaret BL, Beller GA (2010) Clinical nuclear cardiology: state of the art and future directions. Clin Nucl Cardiol State Art Futur Dir 12:1–878. https://doi.org/10.1016/C2009-0-53360-0
45. Tayebi T et al (2021) Biofabrication of chitosan/chitosan nanoparticles/polycaprolactone transparent membrane for corneal endothelial tissue engineering. Sci Rep. https://doi.org/10.1038/S41598-021-86340-W
46. Coleman MM, Zarian J (1979) Fourier-transform infrared studies of polymer blends. II. Poly(ϵ-caprolactone)–poly(vinyl chloride) system. J Polym Sci Polym Phys Ed 17(5):837–850. https://doi.org/10.1002/POL.1979.180170509
47. Hu T, Hu M, Gao B, Li W, Wang X (2018) Screening surface structure of mxenes by high-throughput computation and vibrational spectroscopic confirmation. J Phys Chem C 122(32):18501–18509. https://doi.org/10.1021/ACS.JPCC.8B04427/SUPPL_FILE/JP8B04427_SI_001.PDF
48. Korniienko V et al (2021) Functional and biological characterization of chitosan electrospun nanofibrous membrane nucleated with silver nanoparticles. Appl Nanosci. https://doi.org/10.1007/s13204-021-01808-5
49. Fan H, Guo Z (2020) Bioinspired surfaces with wettability: biomolecule adhesion behaviors. Biomater Sci 8(6):1502–1535. https://doi.org/10.1039/C9BM01729A
50. Lin WC, Razali NAM (2019) Temporary wettability tuning of PCL/PDMS micro pattern using the plasma treatments. Mater 12:644. https://doi.org/10.3390/MA12040644
51. Basara G et al (2022) Electrically conductive 3D printed $Ti_3C_2T_x$ MXene-PEG composite constructs for cardiac tissue engineering. Acta Biomater 139:179–189. https://doi.org/10.1016/J.ACTBIO.2020.12.033
52. Liang Y, Mitriashkin A, Lim TT, Goh JCH (2021) Conductive polypyrrole-encapsulated silk fibroin fibers for cardiac tissue engineering. Biomaterial 276:121008. https://doi.org/10.1016/J.BIOMATERIALS.2021.121008
53. Sundaram A, Francis BM, Dhanabalan SC, Ponraj JS (2021) Transition metal carbide—MXene. Handb carbon-based nanomater. Elsevier, pp 671–709
54. Sang M et al (2022) Advanced MXene/shear stiffening composite-based sensor with high-performance electromagnetic interference shielding and anti-impacting Bi-protection properties for smart wearable device. Chem Eng J. https://doi.org/10.1016/J.CEJ.2022.135869
55. Gil-Cabrerizo P, Scacchetti I, Garbayo E, Blanco-Prieto MJ (2023) Cardiac tissue engineering for myocardial infarction treatment. Eur J Pharm Sci. https://doi.org/10.1016/j.ejps.2023.106439
56. Yu Z et al (2023) 3D conductive scaffolds of MXene@PCL with high conductivity and small line width fabricated by electric-field-driven jet 3D printing and electrostatic self-assembly. Mater Today Commun. https://doi.org/10.1016/j.mtcomm.2023.105704
57. Shokrollahi P, Omidi Y, Cubeddu LX, Omidian H (2023) Conductive polymers for cardiac tissue engineering and regeneration. J Biomed Mater Res Part B Appl Biomater. https://doi.org/10.1002/jbm.b.35293
58. Akbarzadeh A, Sobhani S, SoltaniKhaboushan A, Kajbafzadeh AM (2023) Wholeheart tissue engineering and cardiac patches: challenges and promises. Bioengineering. https://doi.org/10.3390/bioengineering10010106
59. Wang B et al (2023) Functional acellular matrix for tissue repair. Mater. Today Bio 18:100530. https://doi.org/10.1016/j.mtbio.2022.100530
60. Salaris V, López D, Kenny JM, Peponi L (2023) Hydrolytic degradation and bioactivity of electrospun PCL-MG-NPS fibrous mats. Molecules. https://doi.org/10.3390/molecules28031001
61. Dias JR, Sousa A, Augusto A, Bártolo PJ, Granja PL (2022) Electrospun Polycaprolactone (PCL) degradation: an in vitro and in vivo study. Polymers (Basel). https://doi.org/10.3390/polym14163397
62. Ye G et al (2020) Mussel-inspired conductive Ti_2C-cryogel promotes functional maturation of cardiomyocytes and enhances repair of myocardial infarction. Theranostics 10(5):2047–2066. https://doi.org/10.7150/THNO.38876
63. Rafieerad A et al (2019) Quantum dots: application of Ti_3C_2 MXene quantum dots for immunomodulation and regenerative medicine (Adv Healthcare Mater 16/2019). Adv Healthc Mater 8(16):1970067. https://doi.org/10.1002/ADHM.201970067
64. Rafieerad A et al (2021) Fabrication of smart tantalum carbide Mxene quantum dots with intrinsic immunomodulatory properties for treatment of allograft vasculopathy. Adv Funct Mater 31(46):2170341. https://doi.org/10.1002/ADFM.202170341
65. Asaro GA et al (2023) MXene functionalized collagen biomaterials for cardiac tissue engineering driving iPSC-derived cardiomyocyte maturation. Npj 2D Mater Appl 71(1):1–13. https://doi.org/10.1038/s41699-023-0409-w

66. Salmi MS, Ahmed U, Aslfattahi N, Rahman S, Hardy JG, Anwar A (2022) Potent antibacterial activity of MXene-functionalized graphene nanocomposites. RSC Adv 12(51):33142–33155. https://doi.org/10.1039/D2RA04944A
67. Santos X et al (2022) Antibacterial capability of MXene ($Ti_3C_2T_x$) to produce PLA active contact surfaces for food packaging applications. Membranes Basel 12(11):1146. https://doi.org/10.3390/MEMBRANES12111146
68. Rasool K, Helal M, Ali A, Ren CE, Gogotsi Y, Mahmoud KA (2016) Antibacterial activity of $Ti_3C_2T_x$ MXene. ACS Nano 10(3):3674–3684. https://doi.org/10.1021/ACSNANO.6B00181
69. Shan G, Ding Z, Gogotsi Y (2023) Two-dimensional MXenes and their applications. Front Phys. https://doi.org/10.1007/s11467-022-1254-2